

# DEVELOPMENT OF POWER CONVERTER FOR HIGH POWER PIEZOELECTRIC MOTORS

Thomas SCHULTE, Hugues D. NJIENDE, Norbert FRÖHLEKE

Institute of Power Electronics and Electrical Drives  
University of Paderborn, FB14/LEA  
33095 Paderborn

## Abstract

Several types of piezoelectric motors are known to deliver few watts of mechanical output power. This paper deals with the design and development of a LLCC-resonant converter for a novel type of high power piezoelectric motor of up to 4kW mechanical power being used in avionics. The development of a laboratory power supply became necessary, since suitable power supplies for testing the novel piezoelectric motor during its breadboard stage are not available on the market.

The general function of the LLCC-resonant converter which also provides a DC-offset voltage for avoiding depolarisation problems is described, implementation highlights and especially the inductor design are outlined.

## 1 Introduction

Several types of piezoelectric motors are known, like traveling wave type ultrasonic motor or inchworm motor, etc., see [1]. To the authors best knowledge the most powerful up to date piezoelectric motors deliver about 20 Watt of mechanical output power at maximum efficiency of about 20%.

Within the scope of the EUREKA-project PAMELA (Piezo Active Motor for more ELectrical Aircraft) the development of a high power piezoelectric motor (HPM) is aimed by company SAGEM SA. The HPM is designed for replacing hydraulic actuators for operating secondary flight control surfaces in aircrafts. Since piezoelectric actuators (motors) combine such features as high power and torque (or force) density especially at low speed and low electromagnetic interferences, they are suitable for being used in avionics.

The novel HPM is designed to generate a mechanical output power of about 4kW. The total electrical input power is about 18kW active power<sup>1</sup> and from 50 to 80kVAr capacitive power. This data reflects a new class of piezoelectric actuators. The operating fre-

quency is about 20kHz and the motors voltage amplitudes are in a range of up to 540V<sub>p</sub>. Additionally the HPM should be fed with almost unipolar voltages to avoid depolarisation of the piezoelectric ceramic. Therefore a DC-offset voltage must be superimposed on the supplied AC-operating voltage.

Currently, adequate power supplies are not commercially available. This paper deals with the development of a provisional power supply for testing the HPM under laboratory conditions. In chapter 2 the general operation of LLCC resonant converters is outlined. The realisation problems including the inductor design using a CAE tool are discussed in chapter 3, while in chapter 4 experimental results are presented.

## 2 LLCC-Resonant converter

Different types of power converters have been discussed for feeding piezoelectric motors. Voltage fed resonant converters with half- or full-bridge topology turned out as most suitable. In [2] LLCC-resonant circuits are proposed for shaping the transfer function so that almost fixed output voltages are generated and in [5] the LLCC-resonant converter is discussed with respect to its advantages in conjunction with a control system.

Fig. 1 depicts the general topology (a) (full-bridge) and the frequency response of a LLCC-resonant converter (c), which shows a gain of almost 0dB and a phase of almost 0deg around the nominal operating frequency  $\omega_{sN}$ .  $C_{pN}$  is the nominal capacitance of the piezoelectric actuator. Since piezoelectric motors are operated within a relative small bandwidth (20kHz  $\pm$ 1kHz for HPM), the LLCC-resonant technique provides almost impressed motor voltages in a sufficient wide frequency range. In Fig. 1c the load parameters  $C_p$  and  $R_p$ , representing a simple passive test load, are varied in order to simulate equivalent behaviour of the HPM with temperature ( $C_p$ ) or load ( $R_p$ ) variation.

In Chapter 1 it is mentioned, that the motor must be fed with an additional DC-offset voltage. One simple and reliable measure for providing a DC-offset voltage in a range of the AC-voltage amplitude is to use the DC-

---

1. The efficiency of piezoelectric motors is usually less than 25%.

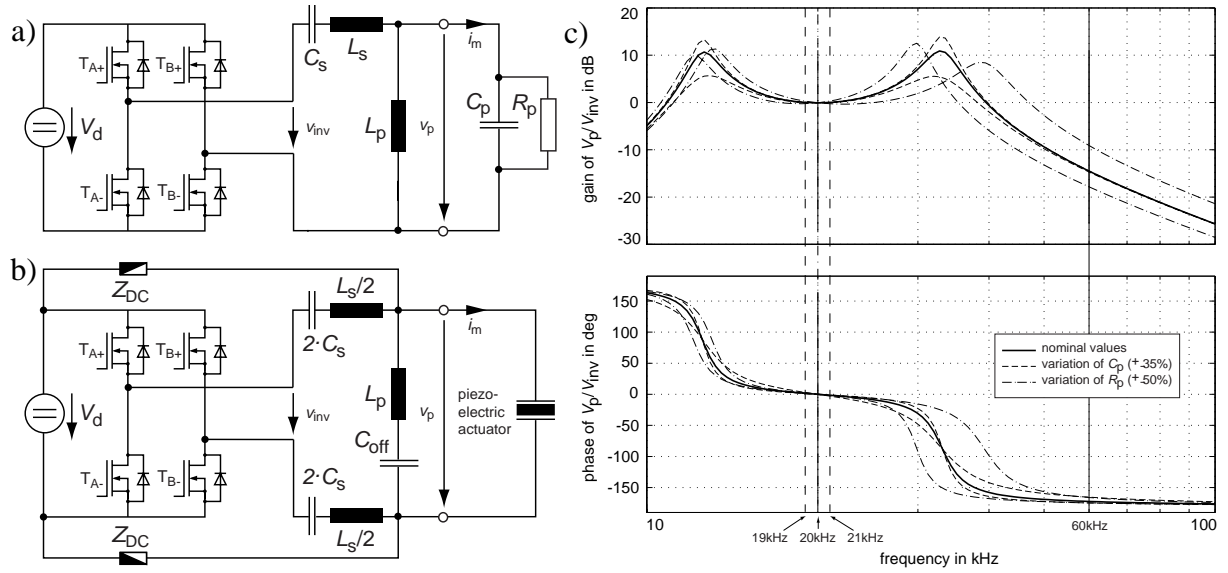


Fig. 1: Topology of a conventional LLCC-resonant converter (a), topology of a LLCC-resonant converter with DC-offset voltage (b) and frequency responses of LLCC resonant tanks (c).

bus voltage directly linked to the output (see Fig. 1b) via resistors  $R_{DC}$  and/or inductors  $L_{DC}$  (marked by  $Z_{DC}$  in Fig. 1b) for decoupling the AC part. The converter stage is decoupled from the DC-offset voltage by series capacitors  $C_s$  distributed on both lines of the LLCC-resonant tanks, while additional capacitor  $C_{off}$  is blocking the DC-voltage from parallel coil  $L_p$ . In order to minimize the influence of the blocking capacitor capacitance  $C_{off}$  must be relatively high in comparison to the other components. Since only leakage current must be fed to the resonant circuits by the DC link, the realisation of  $R_{DC}$  ( $L_{DC}$  resp.) is no problem. In the framework of this project resistive decoupling by  $R_{DC}$  is used only.

### 3 Power converter for HPM

#### 3.1 Topology and Total System

Fig. 3 shows the total topology of the system. The HPM has two times two phases (1a, 1b and 2a, 2b); the phases with index 1 belong to the *main mode* and phases with index 2 belong to the *auxiliary mode*. Each phase of the resonant converter feeds two series connected sets of piezoelectric actuators.

The AC-voltages of phases with index a and index b of each mode show temporal phase shifts of  $\pi$ , see Fig. 2. The control of the HPM relies on a variation of frequency  $f_s$ , temporal phase angle  $\phi_{el}$  (between 1a and 2a, 1b and 2b respectively) and duty cycles  $\beta_1$  (for 1a and 1b) and  $\beta_2$  (for 2a and 2b).

Phases 1a and 1b of the main mode are fed by two independent full bridge inverter stages, while phase 2a and 2b of the auxiliary mode are driven by one com-

mon inverter stage via two independent resonant circuits, see Fig. 3. The DC bus is realized by direct rectification of the 3 phases 400V<sub>RMS</sub>, 50Hz main<sup>2</sup>. Relative high capacitance value for  $C_d$  and input inductors  $L_d$  for ensuring a low ripple on the DC bus voltage  $V_d$ . Due to the input inductors  $V_d$  becomes load dependent and ranges from 520V to 565V. The amplitude of  $v_{pi}$  is calculated by

$$\hat{v}_{pi} = V_d \cdot \frac{4}{\pi} \cdot \sin\left(\frac{\beta_i}{2}\right). \quad (1)$$

Thus, the maximum amplitude  $\hat{v}_{pmax} = 4/\pi \cdot V_d$  is about 720V and for limiting the motors voltages  $v_{pi}$   $\beta_i$  must be limited to about 120°.

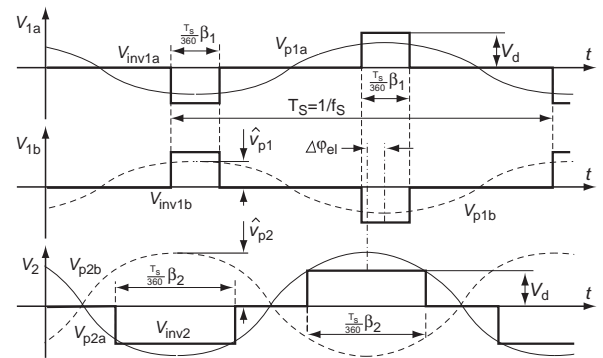


Fig. 2: Principle waveforms of motor and inverter voltages. Due to the behaviour of the LLCC-resonant circuits the fundamental components of the inverters output voltages  $v_{inv}$  and corresponding motors voltages  $v_p$  are equal.

2. In aircrafts the main supply is via 3 phases with 115V<sub>RMS</sub>, 300Hz, affected by heavy voltage and frequency variations.

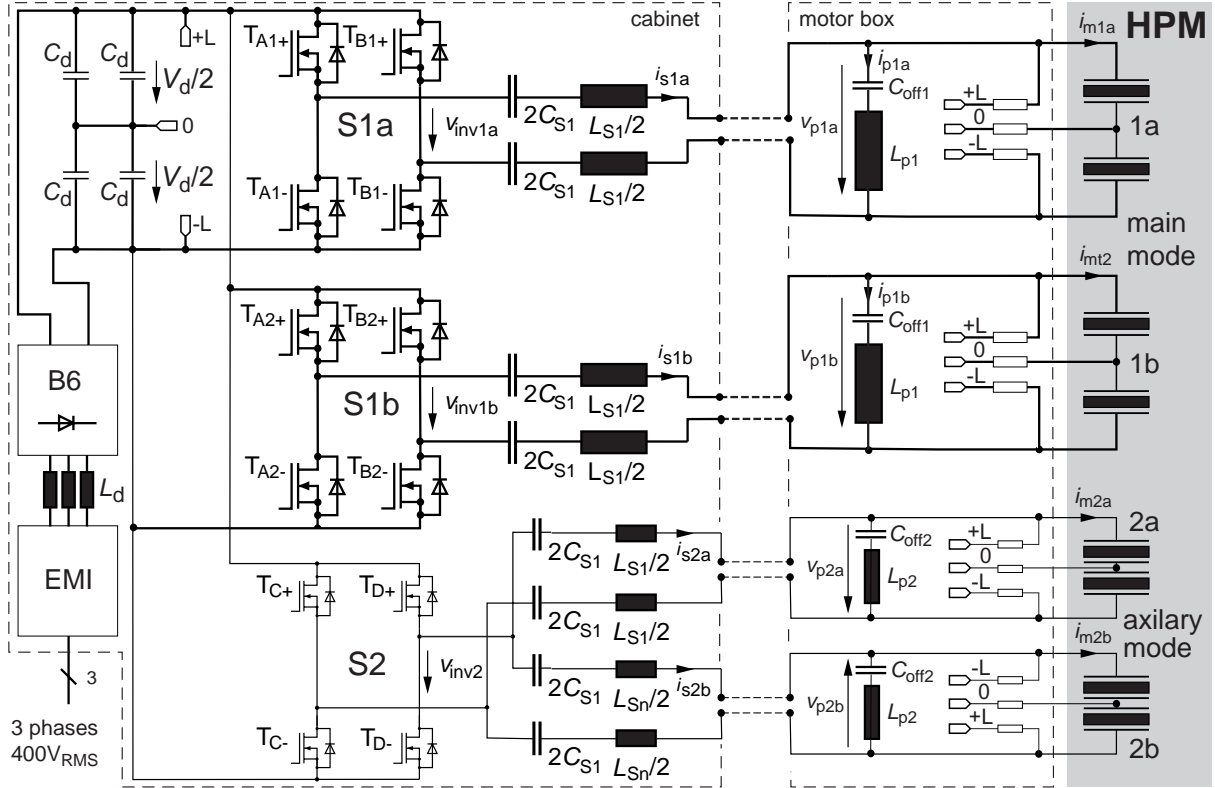


Fig. 3: Topology of two times two phases 80kVAr LLC-resonant converter

### 3.2 Power Converter for HPM

In Table 1 the parameters of both phases are listed. The realisation of the auxiliary mode circuit is no problem but of main mode circuit. One problem is the large variation of the load parameters. The active power is

	phase 1 (each a and b)	phase 2 (each a and b)
$P$	9kW	160W
$C_{pN}$	1.75 $\mu$ F	75nF
$L_p$	38.8 $\mu$ H	908 $\mu$ H
$C_s$	1.75 $\mu$ F	75nF
$L_s$	31.7 $\mu$ H	792 $\mu$ H
$C_{off}$	24 $\mu$ F	1 $\mu$ F

Table 1: Nominal parameters of resonant circuits.

varied while different mechanical load is applied to the system. Reactive power is varied since  $C_p$  depends on the operating temperature. The HPM is operated in a wide temperature range and therefore the power converter must match a wide variation of  $C_p$  (about

$\pm 35\%$ ). Additionally the operating frequency is varied in a range of  $\pm 1$ kHz. While the frequency response of the system in Fig. 1c shows almost fixed gain and phase values independent from frequency,  $C_p$  and  $R_p$ , we observe heavy variation of the admittance curves in Fig. 4 (calculated for the main mode with passive  $C_p - R_p$  test load).

At the nominal operating point A the admittance value is low and the phase angle is  $0^\circ$ . This means active

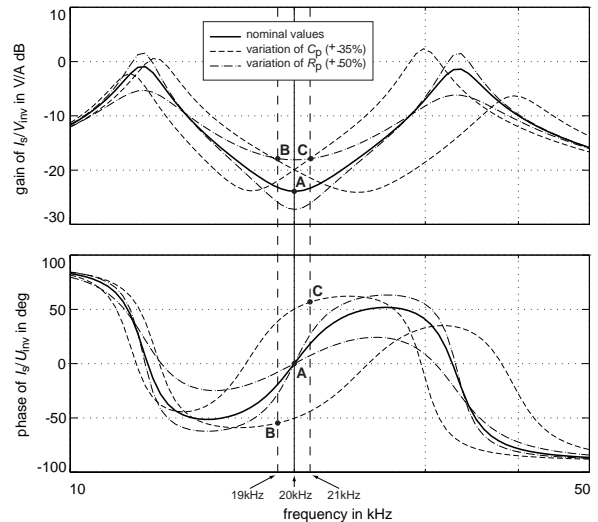


Fig. 4: Admittance curves of LLC resonant tanks.

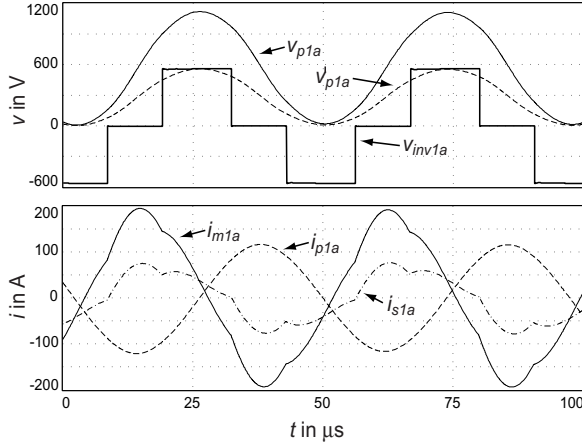


Fig. 5: Simulation of main mode 1a in worst case operation (operation point C).

power feeding by the inverter stage only and a relative low current through the series components  $C_s$  and  $L_s$ . But in worst case operating points **B** and **C** the admittance values are more than doubled and the phase angle is about  $\pm 60^\circ$  implying that high reactive power must be fed by the inverter stage.

series current $i_{s1a,eff}$	55.3 A
current through parallel coil $i_{p1a,eff}$	84.0 A
motor current $i_{m1a,eff}$	129.6 A
AC motor voltage $v_{p1a,AC,eff}$	398 V
DC motor voltage $v_{p1a,DC}$	561 V

Table 2: Load values of main mode 1a at worst case operation (operation point C).

Fig. 5 shows simulation results of main mode 1a in operation point **C**, which turned out as worst case with respect to total losses. Corresponding load values calculated from simulation results are stated in Table 2. The AC part of the motor voltages  $v_{p1a}$  is almost sinusoidal and in phase with the fundamental component of inverter voltage  $v_{inv1a}$ . It has  $398V_{eff}$  which results in  $563V_p$  for the AC-amplitude. The DC part is 561 V which results in almost unipolar voltage feeding. The total voltage within the system is up to 1100 V. While current  $i_{p1a}$  is almost sinusoidal (due to sinusoidal  $v_{p1a}$ ) the motor current  $i_{m1a}$  and current  $i_{s1a}$  from the inverter stage shows small harmonic distortion.

In summary from above investigation the following points must be taken into account for realization of the provisional power converter for the HPM:

- The design of the highly stressed resonant inductors is difficult. This problem is discussed in more detail in chapter 3.3.

- Since the inductance values of the main mode are very low (s. Table 1) it is important to ensure that inductivities of cables etc. do not disturb the operation of the LLC resonant circuits.
- Insulation capability of components, cables, structure, etc. must be considered carefully.
- Semiconductors (half bridge modules) must be oversized with respect to the nominal current due to the unusual operating conditions and the resulting heat dissipation.

### 3.3 Development of magnetic components

Magnetic components are key components in the LLC-resonant converter, due to their complicated design at high currents and frequency. In order to reduce volume and losses, the behavior of magnetic components has to be accurately predicted and some geometrical parameters be optimized. Therefore the design and optimization tool (CAEOMAG), was used which is integrated in a circuit simulator SIMPLORER. The optimization parameters are usually the core geometry, the air gap length or the layer thicknesses. Using a new approach of optimization: the distance between the air gap and the inner layer is optimized for reducing the losses caused by the air gap fringing and for decreasing hot spot temperatures.

The structure and data flow of CAEOMAG is described in [3]. The design of magnetic components is performed within two steps. Fig. 6 shows the set up of CAEOMAG including iterations loops. Starting from the circuit model a simulation is performed at steady state, generating approximate stress quantities. The pre-optimization algorithm provides data about the expected volume, losses and temperature rise of a fixed core and winding set-up of inductors and transformers and are inputted via a graphical user interface. Thus initial values for a subsequent optional parameter optimization of these components are derived. The component geometry is optimized with respect to desired design objectives which are defined by a weighting vector. This main optimization is represented in the left loop.

Within high current high frequency inductors 2D-air-gap effects are significant. So far winding thickness  $d_{cu}$  and the airgap length  $l_G$  are optimized only by CAEOMAG for reducing winding losses. In order to further reduce the winding losses and particularly the hot spot temperature the distance between air gap and adjacent layer  $h_{un}$  (underlay) is optimized, too, see Fig. 7. All three parameters have to be optimized simultaneously.

In this contribution, the discussion is constrained to the design of the parallel inductors  $L_p$  of the main mode,

since they are most critical. Initially, previous to the main (winding) optimization, an adequate core is selected. It is retained that 4 EE80 cores staked in parallel correspond closest to the calculated optimal core configuration. On the one hand their area product as well as effective cross section and volume are next to the calculated optimized values, on the other hand their winding window is large enough and offers a high potential for further winding and underlay optimization.

It is then proceeded to a precise parameter optimization for layer configuration, conductor thickness and air gap length, without consideration of underlay. The results are stated in Table 3.

Air gap length	6.6mm
Material	litz; 124 strands; 0.1mm; 7 in parallel
Turns per Layer	4;4;4;1 (13 turns in total)
Total Losses	202.26 W
Hot spot	390.47°C

Table 3: Results of inductor optimization.

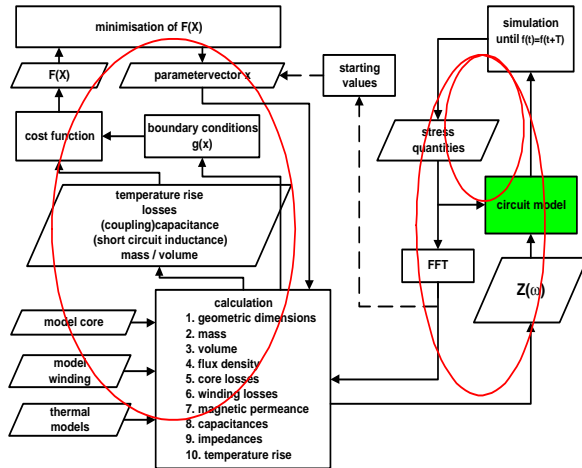


Fig. 6: Setup and iteration loops of CAEOMAG.

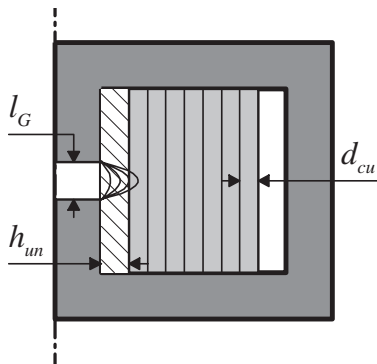


Fig. 7: Geometry of magnetic components.

The temperature (hot spot) of the layer adjacent to the airgap is still too high. Separating the layers from the airgap is one way to minimize this temperature by reducing the field strength in the conductors and therefore decreasing the 2D-losses, [4]. Fig. 8 illustrates the decrease of hot spot temperature ratio  $F_T$  (temperature with underlay divided by temperature without underlay) with increasing the underlay  $h_{un}$ .

Air gap length	4.7mm
Material	litz; 102 strands; 0.1mm; 10 in parallel
Turns per Layer	3;3;3;2 (11 turns in total)
Total Losses	181.86 W
Hot spot	273.86°C
$h_{un}$	~5mm

Table 4: Results of inductor optimization with underlay

Another optimization, using the iteration by underlay  $h_{un}$ , yields the results in Table 4. It depicts the enhancement of the inductor with adequate winding configuration and thickness. The underlay clearly leads to a decrease of hot spot temperature. Note, that due to the optimization procedure the layer configuration of inductors in Table 3 and 4 differ though inductance and current are equal.

For the technical implementation some practical aspects are to be taken into consideration:

- The 10 parallel litz wires, longitudinally wound on the core center leg, should not be intermeshed, otherwise it will lead to additional power losses due more pronounced skin and proximity effects.
- Conductor layers should be accurately isolated from each other.
- For appropriate cooling an air channel is built.

Impedance measurements of the inductors  $L_p$  are carried out. Fig. 10 depicts the AC/DC resistance ratio  $F_{AC}$ . Up to 25 kHz measured and calculated resistance ratio match very well. Above 25 kHz there is a divergence which can partly be allocated to the differences

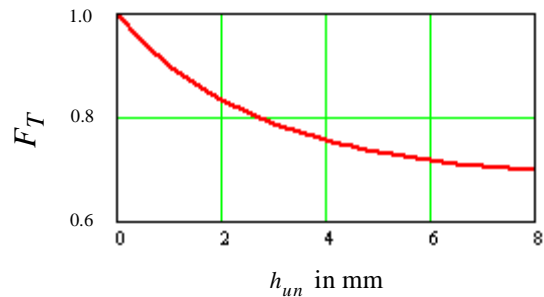


Fig. 8: Hot spot temperature ratio of inductor.

between modelling assumptions and practical layout of the physical winding with 10 parallel wound litz wires.

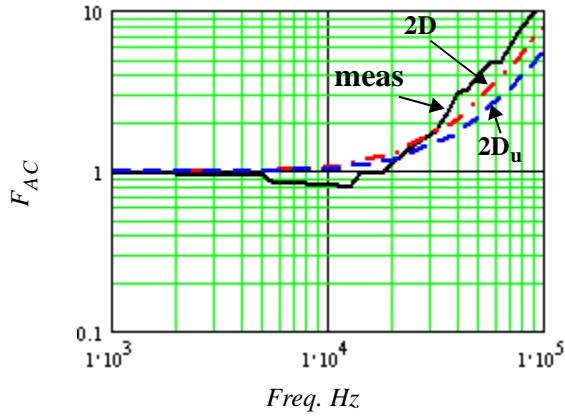


fig. 9: Measured AC/DC resistance ratio of inductor

## 4 Measuring results

First measurements are performed by use of a  $R_p$ - $C_p$ -test load (without HPM). Fig. 10a shows a measurement with applied DC-voltage. Therefore  $C_p$ -test load can be used, only. Since there is no transformer in the system the output voltages are not independent and can only be determined by subtraction of measuring signals from two probes. The maximum permissible voltage for the probes is 1000V. Thus, the AC-amplitude must not be higher than about  $440V_p$ . The voltage waveforms shows relatively heavy distortion from sinusoidal waveform. This distortions can not be observed when measuring the voltage by means of a special independent scope. Hence, it results from the measuring method and common mode disturbances.

Fig. 10b shows a measurement without applied DC-voltage. The full AC-amplitude for  $v_{p1a}$  of  $540V_p$  is driven and load resistor  $R_p$  is introduced. Since no low inductive resistor ( $R_p = 16.2\Omega$ ,  $P = 9kW$ ) was available an additional rectifier is introduced. Due to the inherent inductance of the resistor the waveform of current  $i_{r1a}$  measured at the rectifier before  $R_p$  is more rectangular than sinusoidal.

## 5 Conclusion

This paper deals with the development of a LLC resonant converter for high power piezoelectric motors. The general concept, the topology and realisation problems and the design of the magnetic components using a special CAE tool are outlined. Simulation and measurement results are presented.

Commissioning of the power converter in conjunction with the HPM will be performed soon.

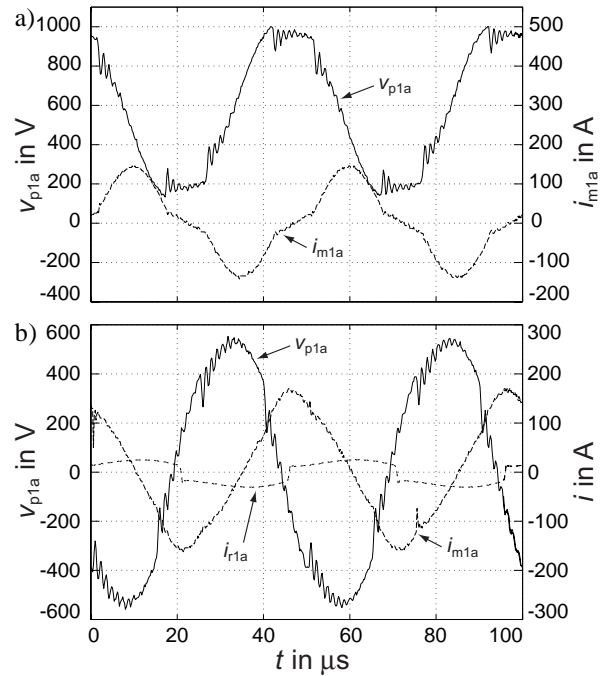


Fig. 10: Measuring results.

## 6 Acknowledgement

The development of the high power LLC resonant converter is a project in cooperation between SAGEM SA (France) and the institute mentioned above in the scope of the EUREKA-project PAMELA which is an European project with partners from industries and universities.

## References

- [1] T. Sashida, T. Kenjo. *An Introduction to Ultrasonic Motors*, Clarendon Press, Oxford 1993.
- [2] F.-J. Lin, R.-Y. Duan, H.-H. Lin. An Ultrasonic Motor Drive Using LLC Resonant Technique. *Proc. of PESC'99*, Vol. 2, pp. 947-952.
- [3] P. Wallmeier, N. Fröhleke, D. Hahm, H. Mundinger. Integrating magnetic component design and optimization into circuit simulator SIMPLORER. *Proc. of Power Conversion and Intelligent Motion Conf. (PCIM) 2000*, Nürnberg, June 2000, pp 533-538.
- [4] N. H. Kutkut. Minimizing winding losses in foil winding using field shaping techniques. *Proc. of PESC'97*, Vol. 5, pp. 634-640.
- [5] T. Schulte, N. Fröhleke, H. Grotstollen. Control for Ultrasonic Motors with LLC-Resonant Converter. *Proc. of Conf. on New Actuators 2000*, Bremen, Germany, June, 2000, pp. 411-414.